

Hollow cubic CuSe@CdS with tunable size for plasmon induced Vis-NIR driven photocatalytic property

Ning Li^{*abc}, Linping Li^b, Yanping Qiu^b, Xuhui Liu^b, Jiatong Zhang^b, Yangqin Gao^b,

Lei Ge^{*ab}

^a Key Laboratory of Heavy Oil Processing, China University of Petroleum Beijing,

No. 18 Fuxue RD, Beijing 102249, China

^b Department of Materials Science and Engineering, College of New Energy and Material, China University of Petroleum Beijing, No. 18 Fuxue RD, Beijing 102249,

China State

^c Beijing Key Laboratory of Failure, Corrosion, and Protection of Oil/Gas Facilities

*corresponding author, E-mail address: wubian.good@163.com (N. Li),

gelei08@sina.com (L. Ge)

Abstract:

The rational design of dimension and geometry of plasmonic semiconductor cocatalyst is vitally important to the efficiently utilizing of near-infrared light (NIR) and the superior photocatalytic hydrogen generation. Herein, hollow cubic CuSe@CdS composites with different size and strong localized surface plasmon resonance (LSPR) were prepared by selenizing size-tunable Cu₂O templates and loading CdS nanoparticles. The size of hollow cubic CuSe can affect the surface area and the conduction band potential by the size effect, regulating the carrier behavior of the CuSe@CdS heterojunction. The CuSe@CdS composites perform enhanced and wide absorption in full spectrum due to the LSPR effect of CuSe. Meanwhile, the composites show excellent photocatalytic hydrogen capacity in full spectrum in 0.35 M Na₂S / 0.25 M Na₂SO₃ sacrificial reagent solution: The best hydrogen production rate of CSCE2 is 1.518 mmol g⁻¹h⁻¹ (5.54 times higher than CdS) under Vis light (780 > λ > 420 nm)

irradiation, and $0.28 \text{ mmol g}^{-1}\text{h}^{-1}$ under NIR light ($\lambda > 780 \text{ nm}$) illumination. Interestingly, the photocatalytic activity for H_2 under Vis-NIR light ($\lambda > 420 \text{ nm}$) is about 3 times (up to $4.45 \text{ mmol g}^{-1}\text{h}^{-1}$) higher than that without NIR light assistance, due to the photothermal effect. Various analyses and DFT calculations demonstrate that the p-n heterojunction is formed in the composites consisting of p-type CuSe and the n-type CdS, which achieves efficient carrier transfer and separation under the synergistic effect of size effect and photothermal effect. Additionally, the expansion of the photocatalytic performance to NIR range is mainly due to the “hot-electron” injection mechanism induced by the LSPR effect of CuSe. The reasonable design coupled with the plasmonic materials offers a new path to achieve the high-efficient conversion of solar energy to hydrogen energy.

1. Experimental section

1.1. Material Characterizations.

The crystal structure of the samples was characterized by a Bruker D8 Advance X-ray diffractometer (XRD) using Cu K radiation, with the diffraction angle from 5 to 90° . The morphology and sizes were examined by Field-emission transmission electron microscopy (TEM) and field-emission scanning electron microscopy (SEM) using FEI Tecnai G2 F20 and FEI SU8010, respectively. X-ray photoelectron spectroscopy (XPS) analyzing the chemical compositions was obtained by ESCALAB 250XI. The UV-Vis diffuse reflectance spectra (DRS) were obtained with the UV-4100 spectro-photometer using BaSO_4 as the reflectance standard.

The electrochemical impedance spectroscopy (EIS) was tested in a CHI 760e electrochemical system using a three-electrode system, using an open-circuit potential without light irradiation in the frequency range of $0.1\text{--}10^5 \text{ Hz}$ and $0.5 \text{ M Na}_2\text{SO}_4$ electrolyte, where Pt wire as counter electrode, Ag/AgCl as reference electrode and ITO coated by as-prepared photocatalysts as working electrode. The working electrodes were prepared as follows: 5 mg of photocatalyst was dispersed in 0.25 ml ethanol, 1 ml H_2O and $10 \mu\text{l}$ 5% Nafion solution by sonicating for 30 min . Finally, $80 \mu\text{l}$ of the above mentioned suspension was deposited on the ITO and dried at 60°C . The photocurrent

measurements were conducted in the 0.5 m Na₂SO₄ solution with chopped illumination. The light resource was provided by a 500 W Xe arc lamp (PerfectLight) through an AM 1.5G filter and using a thermopile detector (Photoelectric Instrument Factory of Beijing Normal University) to adjust the light intensity to 100 mW m⁻². Mott–Schottky experiments were conducted at the frequency of 1 KHz with the amplitude of 5 mV under 0.5 M Na₂SO₄ solution.

1.2. Photocatalytic H₂ Evolution.

Perfectlight Labsolar IIAG system was used to measure the photocatalytic hydrogen evolution with different wavelength filters. 8.4 g of Na₂S and 3.15 g of Na₂SO₃ were added to 300 ml of quartz photoreactor and dissolved in 100 ml of deionized water. Then, add 50 mg of the sample and dissolve it by ultrasound. After adding a magnet, the quartz photoreactor was sealed with a rubber ring and a quartz cap under the action of a vacuum ester. Connected with a closed gas circulation system, the quartz photoreactor was connected to the circulating water installation to maintain a temperature of 4 °C throughout the reaction. The entire system is evacuated for more than 30 minutes to ensure complete closure before starting the irradiation. The light source (PLS-SXE 300 UV Xe arc lamp) was 1 dm over the reactor to illuminate the reactants with light intensity of 32 mW/cm². In the case of argon as a carrier gas, gas chromatography (Beifen 3420 A, TCD) is utilized to analyze the composition and content of the evolved gas. For the recycling tests of photocatalytic H₂ evolution, after finishing each cycle, the entire system is evacuated for more than 30 minutes to ensure complete vacuum without residual H₂, before starting a new recycling test of photocatalytic H₂ evolution, and the reaction solution in quartz photoreactor needless to do other processing.

1.3. DFT calculation

We performed electronic structure calculations through density functional theory (DFT) in the Vienna ab initio simulation program (VASP) package code. The energy cutoff of 400 eV was used for plane-wave expansion of electron wave functions based

on the convergence test. The Perdew, Burke, and Ernzerhof (PBE) exchange-correlation functional within a generalized gradient approximation (GGA) was employed. The Brillouin zone was sampled using a Gamma-centered scheme with a $(2 \times 4 \times 1)$ k-point grid. The calculations were iterated until the total energy converged to 10^{-6} eV. The atomic positions were relaxed until the force on each atom was less than 0.05 eV/Å. The vacuum gap thickness was set to be 15 Å for CuSe (001) and CdS (010).

2. Results and discussion

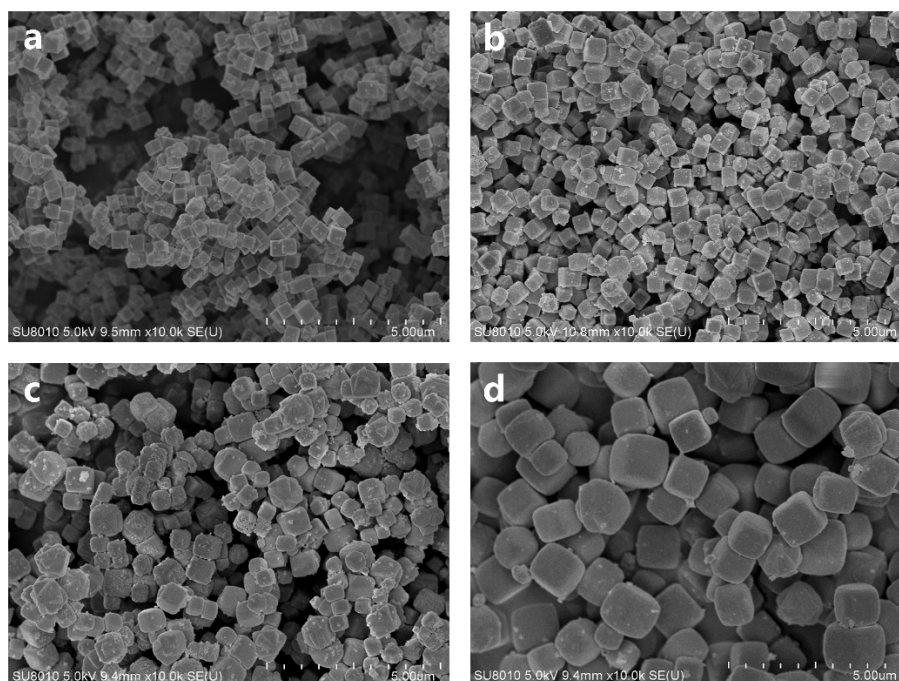


Fig. s1. SEM images of Cu₂O with different sizes by adjusting the amount of NaOH: (a) Cu₂O-1, (b) Cu₂O-2, (c) Cu₂O-3 and (d) Cu₂O-4.

Table s1. Amounts of reagents and the reaction conditions used for synthesizing various sizes of Cu₂O nanocubes.

Sample	Average size (nm)	CuSO ₄ ·5H ₂ O	NaOH	C _{NaOH} /C _{Cu}	Ascorbic acid	Dropping acceleration of ascorbic acid solution (drops/s)	Sodium citrate
Cu ₂ O-1	120		0.114M	7.6		1	
Cu ₂ O-2	360	0.015M	0.25M	16.7	0.03M	1	0.005M
Cu ₂ O-3	600		0.564M	37.6		3	
Cu ₂ O-4	990		0.789M	52.6		3	

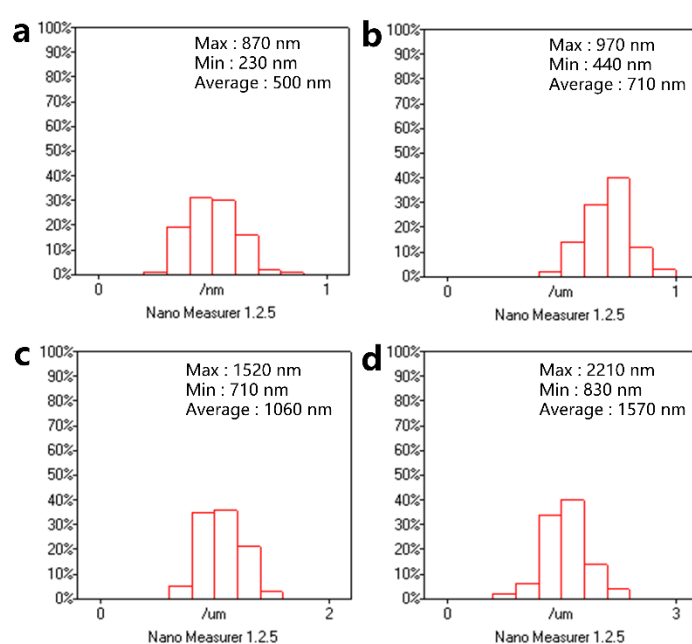


Fig s2. The size normal distribution diagram of different CuSe samples: (a) CuSe-1, (b) CuSe-2, (c) CuSe-3, (d) CuSe-4.

Table s2. The results of N₂ adsorption-desorption isotherm of different samples.

Sample	CuSe-1	CuSe-2	CuSe-3	CuSe-4
BET surface area (m ² g ⁻¹)	14.9876	45.5660	14.5338	7.8069
Pore volume (cm ³ g ⁻¹)	0.063556	0.140471	0.059526	0.013968
Pore size (nm)	27.5219	11.0821	40.4756	48.8049

Table s3. Ratio of CuSe (JCPDS 34-1017) and Cu_{2-x}Se (JCPDS 06-0680) phase contents in XRD patterns analysed by the RIR value method

Sample	Klockmannite -CuSe(Wt%)	Berzelianite -Cu _{2-x} Se(Wt%)
CuSe-1	79.6	20.4
CuSe-2	77.7	22.3
CuSe-3	75.4	24.6
CuSe-4	90.9	9.1

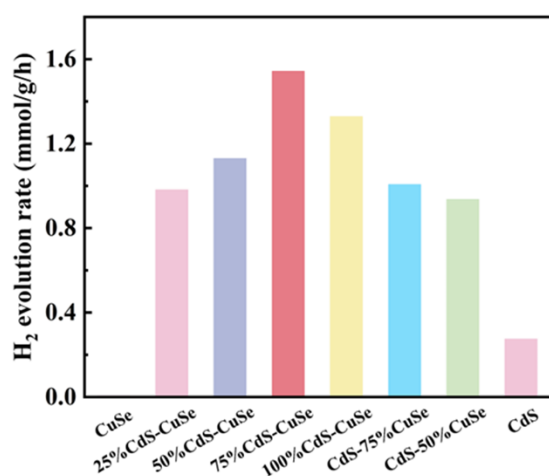


Fig s3. Photocatalytic H₂ evolution rate of CuSe-2@CdS composites with different ratios

Table s4. Irradiation intensity at each point in the measurement of apparent quantum efficiency at 420 nm

Point	Center	1	2	3	4	5	6
Vis-driven	30.5	2.0	2.1	1.8	2.1	2.0	2.1
Vis-IR-driven	31.2	2.1	2.0	2.0	2.1	2.0	2.0

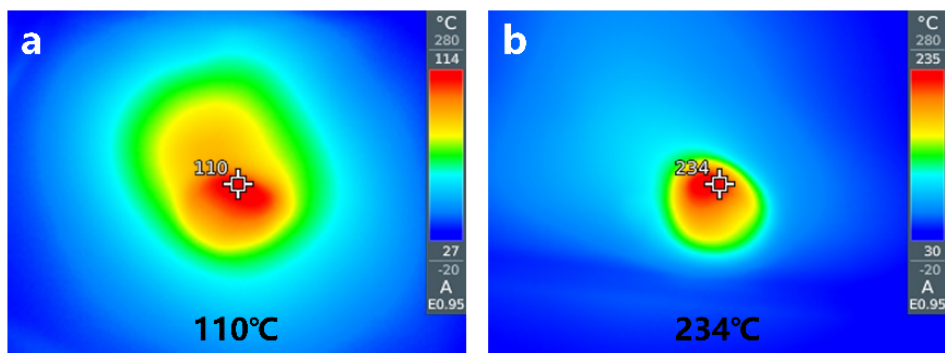


Fig s4. Infrared photos of (a) CdS (b) CSCE2 under Vis-NIR light irradiation.